Communication

Metrics for Localized Beams and Pulses

Walter Fuscaldo *Member, IEEE,* and Santi C. Pavone, *Member, IEEE*

***Abstract*—Geometric and energy metrics are here proposed to gauge the confinement properties of localized electromagnetic beams (e.g., Bessel beams) and pulses (e.g., X-waves) in both the nondispersive and dispersive cases. As is well known, the frequency superposition of Bessel beams sharing the same axicon angle leads to the generation of tightly bounded wavepackets, namely X-waves, with remarkable spatio-temporal confinement properties. In the nondispersive case, the axicon angle does not change with frequency, and these features can be predicted by closed-form expressions. Remarkably, it is found that the volumetric confinement of such pulses can be optimized for a specific axicon angle. Since the geometric metrics do not account for the unavoidable presence of energy tails outside the main spot, energy metrics are here introduced and compared with the purely geometric definition. Finally, the dispersive case is investigated, accounting for the typical wavenumber dispersion of radial waveguides. As a result, the axicon angle changes with the frequency, and fundamental limits exist for the maximum theoretical fractional bandwidth. Interestingly, design criteria based on approximate analytical expressions are derived to optimize the confinement, even in the dispersive case.**

***Index Terms*—Bessel beams, X-waves, localized waves, radial waveguides, dispersion, diffraction, near-field focusing.**

I. Introduction

RECENTLY, several efforts have been made to improve the focusing capabilities of radiating devices in the near-field region. The interest in this topic is motivated by the broad range of applications, such as wireless links, secure communications, medical imaging, etc., where it is important to focus electromagnetic waves with millimeter resolution [1].

In this context, localized waves [2] are gaining much attention thanks to their remarkable limited-dispersion and limited-diffraction properties. As a matter of fact, the most known representatives of the monochromatic and polychromatic versions of localized waves, i.e., Bessel beams and X-waves, respectively, can be generated through different classes of radiators [3], such as axicon lenses [4], [5], radial waveguides [6]–[15], annular slits [16], [17], and flared coaxial cables [18].

Among these solutions, radial waveguides are particularly attractive thanks to their low profile, low cost, and ease of fabrication [1]. However, differently from lens-like solutions [18], radial waveguides are intrinsically affected by wavenumber dispersion [13]–[15], which in turn determines the so-called *cone dispersion* [19], [20], an unavoidable physical phenomenon that adversely affects the focusing capability of the resulting X-waves, as recently confirmed by a microwave experiment [15].

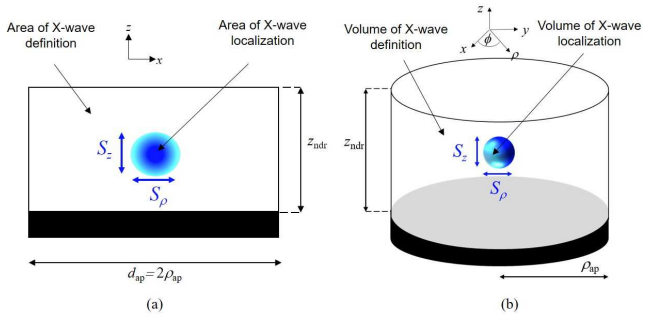

Fig. 1. (a) Two-dimensional (2-D) view and (b) three-dimensional (3-D) view of an X-wave launched through a planar aperture. In (a) and (b) the geometric metrics are defined over a 2-D and a 3-D space, respectively.

The first theoretical analysis of X-waves characterized by the wavenumber dispersion of radial waveguides appeared in [13]. There, exact and approximate analytical expressions to evaluate the spot size of nondispersive and dispersive X-waves were provided. In addition, a geometric metric was first introduced to measure the localization properties of X-waves. However, the geometric metric in [13] has several limitations: *i)* it only applies to nondispersive X-waves; *ii)* it neglects the three-dimensional (3-D) nature of X-waves; *iii)* it does not provide any information about the *energetic confinement* of X-waves.

In this work, moving from [13], we thoroughly assess an in-depth analysis of both nondispersive and dispersive X-waves. Starting from the localization properties of nondispersive X-waves, we review and extend the main results of [13] to account also for the volumetric 3-D case (Section II). This investigation reveals that an optimal design parameter exists that allows for achieving the highest volumetric localization of a pulse in the nondispersive case. Then, the energetic properties of nondispersive X-waves are investigated (Section III). Unfortunately, the definition of an energy metric, even in the nondispersive case, does not allow for closed-form expressions. Therefore, the energy metric is numerically evaluated, and compared with the geometric metric to highlight similarities and differences between the two definitions. Finally, the dispersive case is investigated (Section IV) considering the typical wavenumber dispersion that affects radial waveguides commonly used in the microwave/millimeter-wave frequency range for generating localized waves [12]–[15]. Interestingly, an approximate formula is found to optimize the localization of a pulse even in the dispersive case. Conclusions are drawn in Section V.

Manuscript received XXX. xx^xx, xxxx

W. Fuscaldo is with the Department of Information Engineering, Electronics and Telecommunications (DIET), Sapienza University of Rome, 00184 Rome, Italy. (email: walter.fuscaldo@uniroma1.it).

S. C. Pavone is with the Department of Electrical, Electronics, and Information Engineering (DIEEI), University of Catania, Viale Andrea Doria 6, 95125, Catania, Italy. (email: santipavone1@gmail.com).

II. Localization Properties

As originally shown in [16], [21], when a Bessel beam is generated by a finite-size aperture of radius $\rho_{\rm ap}$ (see Fig. 1), its nondiffracting behavior is maintained up to a distance known as nondiffractive range and given by $z_{\rm ndr} = \rho_{\rm ap}\cot\theta$, where θ is the axicon angle, whereas the null-to-null transverse spot size S_ρ is given by [7], [13]

$$S_\rho = j_{0,1}\lambda_0/(\pi\sin\theta), \tag{1}$$

where $j_{0,1} \simeq 2.405$ is the first null of the zeroth-order Bessel function of the first kind [22], and λ_0 is the free-space operating wavelength. It should be noted that S_ρ is a decreasing function of $\theta \in (0, \pi/2)$, thus the theoretical highest transverse resolution is achieved for $\theta = \pi/2$. However, as already pointed out in [7], the choice of θ is subjected to a trade-off between the maximum transverse localization that we can achieve (lower-bounded by λ_0/1.3 which is close to the Abbe diffraction limit for optical systems [23]) and the maximum nondiffracting distance we can reach (theoretically infinite for unlimited radiating apertures), while maintaining such a transverse localization. As a result, one may be interested in minimizing the ratio between S_ρ and $z_{\rm ndr}$ with respect to θ, under the constraint that $S_\rho < d_{\rm ap}$ (a beam whose waist is larger than the aperture diameter $d_{\rm ap} = 2\rho_{\rm ap}$ is of scarce interest in focusing applications). Such a constrained optimization leads to the following condition

$$\theta > \theta_{\rm low} = \arcsin\left[j_{0,1}(2\pi\bar{\rho}_{\rm ap})\right], \quad \bar{\rho}_{\rm ap} := \rho_{\rm ap}/\lambda_0, \tag{2}$$

which lower-bounds the axicon angle to $\theta_{\rm low}$. If one defines the transverse confinement as the ratio between the transverse null-to-null spot size and the aperture diameter $C_\rho = S_\rho/d_{\rm ap}$, (2) corresponds to the condition $C_\rho < 1$.

Different considerations have to be made for nondispersive X-waves, i.e., the weighted frequency superposition of Bessel beams (hereafter always assumed of zeroth-order) sharing the same axicon angle

$$\chi(\rho, z, t) = \int_{\Delta\omega} F(\omega) J_0(k_0 \sin\theta\rho) e^{-jzk_0\cos\theta} e^{j\omega t} d\omega, \tag{3}$$

where ρ and z are the radial and the vertical axis of a cylindrical reference frame (see Fig. 1), t is the time, ω is the radian frequency, k_0 is the vacuum wavenumber, and $J_0(\cdot)$ is the zeroth-order Bessel function of the first kind. It is also worth noting here that (3) neglects diffraction effects due to the aperture truncation. However, experiments on radial waveguides [7], [8], [11] proved that the aperture truncation mildly affects the spot size of localized waves, thus its effect is not accounted for in this analysis.

Differently from Bessel beams, X-waves are both transversely and longitudinally localized. The transverse confinement is defined as for Bessel beams, while the longitudinal confinement is defined as the ratio between the longitudinal null-to-null spot size S_z of the pulse and the nondiffractive range, $C_z = S_z/z_{\rm ndr}$ with S_z given by [13]:

$$S_z = 2\lambda_0/(\Delta\bar{\omega}\cos\theta), \tag{4}$$

where $\Delta\bar{\omega} = \Delta\omega/\omega_0$ is the fractional bandwidth, $\Delta\omega$ and ω_0 being the angular frequency bandwidth and the operating angular frequency, respectively. The definition of C_ρ and C_z allows for measuring the confinement of the pulse main spot with respect to the aperture diameter in the transverse direction, and the nondiffractive range in the longitudinal direction, respectively. The transverse (longitudinal) confinement will thus be upper-limited by $C_\rho(C_z) < 1$ [13]. While the definition of C_ρ is rather intuitive, a few words should be spent on that of C_z. Indeed, we should recall that a nondispersive X-wave retains its nondiffractive character as long as it propagates for $0 \le z \le z_{\rm ndr}$, thus the spot size is well-defined only within this range. This feature, that is peculiar to all localized waves, gives the rationale for the definition of C_z.

For spectrally-flat X-waves (i.e., with $F(\omega) = 1$ for $|\omega - \omega_0| < \Delta\omega/2$ and $F(\omega) = 0$ elsewhere), analytic expressions are found for both C_ρ and C_z [13]:

$$C_\rho = \frac{j_{0,1}}{2\pi\bar{\rho}_{\rm ap}\sin\theta}, \; C_z = \frac{2\sin\theta}{\bar{\rho}_{\rm ap}\Delta\bar{\omega}\cos^2\theta}. \tag{5}$$

It is worth noting here that C_ρ (C_z) is a monotonically decreasing (increasing) function of $\theta \in (0, \pi/2)$. While the condition for the transverse confinement $C_\rho < 1$ of an X-wave dictates a lower bound for θ (see equation (2)), the condition for the longitudinal confinement sets an upper bound

$$\theta < \theta_{\rm up} = \arcsin\left(\Delta\bar{\omega}\bar{\rho}_{\rm ap} - (\Delta\bar{\omega}\bar{\rho}_{\rm ap})^{-1}\right). \tag{6}$$

Equations (2) and (6) are particularly important, since they provide specific guidelines for properly choosing the operating axicon angle of an X-wave launcher for a fixed fractional bandwidth $\Delta\bar{\omega}$ and a given normalized aperture radius $\bar{\rho}_{\rm ap}$.

As suggested in [24], the overall confinement properties of an X-wave can conveniently be visualized on a contour plot where the following figure of merit

$$\mathcal{G}_{\rm 2D} = \begin{cases} 1 & \text{if } \max(C_\rho, C_z) > 1, \\ C_\rho C_z & \text{elsewhere,} \end{cases} \tag{7}$$

is represented as a two-dimensional (2-D) function of the normalized aperture radius $\bar{\rho}_{\rm ap} = \rho_{\rm ap}/\lambda_0$ and the axicon angle θ for a fixed fractional bandwidth (in the example of Fig. 2(a) $\Delta\bar{\omega} = 0.2$). Therefore, the higher is the localization of the pulse, the lower is the value of $\mathcal{G}_{\rm 2D}$ (light color), and vice versa (dark color). As a consequence, one would minimize this figure of merit to improve the confinement properties of a given pulse. Interestingly, if one reports (2) and (6) on the $\bar{\rho}_{\rm ap}\theta$ plane, the boundaries delimiting the region of confinement along both directions are found (see dashed magenta lines in Fig. 2(a)). As commented in [24], the intersection between these two boundaries determines a limit condition,

$$\rho'_{\rm eq} = \frac{j_{0,1}}{2\pi}\sqrt{1 + \frac{4\pi\Delta\bar{\omega}}{j_{0,1}}}, \quad \theta'_{\rm eq} = \arctan\sqrt{j_{0,1}\frac{\Delta\bar{\omega}}{4\pi}}, \tag{8}$$

for equalizing the confinement ratios (in [24] conditions for equalizing the absolute resolutions are reported as well). In Figs. 2(b)–(e), several examples are shown to assess the consistency of the proposed metrics (see caption for details), for the relevant case $\Delta\bar{\omega} = 0.2$ (the role played by the fractional bandwidth has been extensively discussed in [24]).

This article has been accepted for publication in a future issue of this journal, but has not been fully edited. Content may change prior to final publication. Citation information: DOI 10.1109/TAP.2019.2938628, IEEE Transactions on Antennas and Propagation

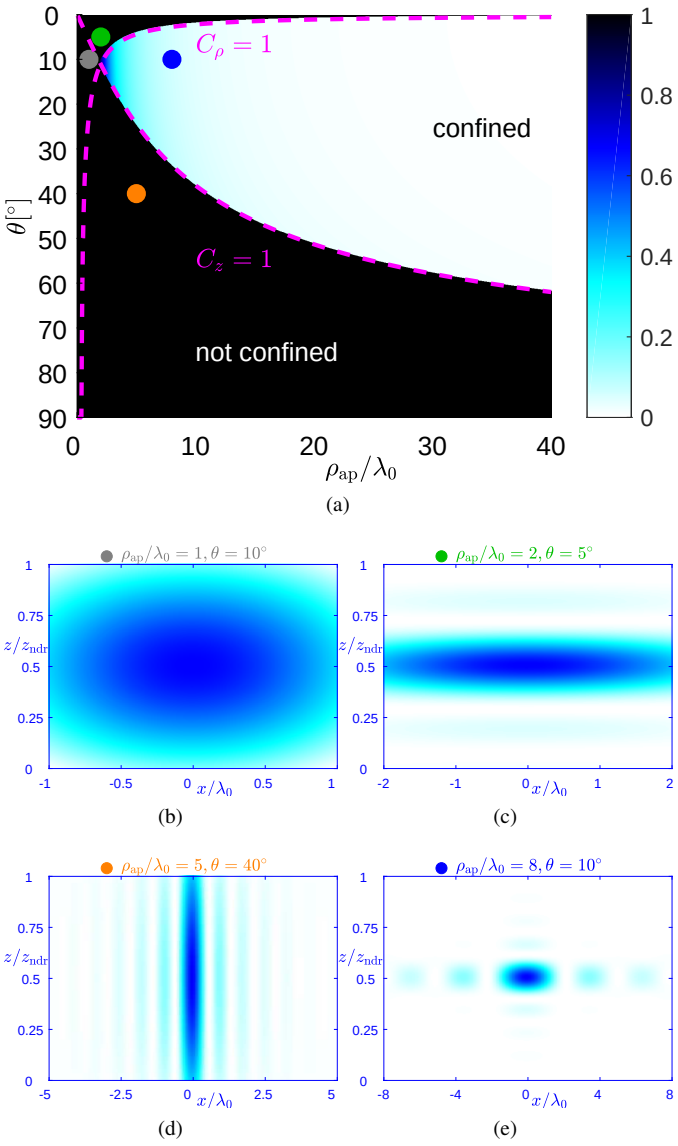

Fig. 2. (a) The geometric metric $\mathcal{G}_{2D}$ vs. ρ_{ap}/λ_0 and θ is shown for $\Delta\omega/\omega_0 = 0.2$ (i.e., a 20% fractional bandwidth). In the black region $C_\rho > 1$ *or* $C_z > 1$, thus the resulting X-wave is not confined along *both* axes. The dashed magenta lines represent the boundaries for which $C_\rho = 1$ (upper boundary) and $C_z = 1$ (lower boundary). The colored dots identify operating points of X-waves whose normalized field intensities $|\chi(\rho, z, t_0)|^2/\max|\chi|^2$ vs. x/λ_0 and z/z_{ndr} have been reported in Figs. 2(b)–(e). The time t is set at the instant t_0 the X-wave peak has reached $z = z_{ndr}/2$. Each colored dot is representative of a typical behavior of an X-wave: an X-wave which is (b) not confined along both directions (grey dot), (c) longitudinally but not transversely confined (green dot), (d) transversely but not longitudinally confined (orange dot), (e) confined along both directions (blue dot).

So far, the confinement properties of an X-wave have been investigated over a 2-D space (x and z). (We note that, due to the azimuthal symmetry of X-waves, the x-axis, is hereafter used in place of the ρ-axis). However, one can easily extend the analysis over a 3-D space by exploiting the azimuthal invariance of the fields, thus considering the domain of interest as the cylinder of radius ρ_{ap} and height z_{ndr}, obtained through a symmetry of revolution around the vertical z-axis. In such a 3-D space, the X-wave main contribution (i.e., the confined electromagnetic pulse without considering the unavoidable pulse tails) can be limited by an ellipsoid with the two semi-axes equal to S_ρ and the other to S_z. Therefore, a figure of merit for the volumetric confinement can be defined as the ratio $\mathcal{G}_{3D} = V_{ell}/V_{cyl}$ between the volumes of the ellipsoid $V_{ell} = (\pi/6)S_\rho^2 S_z$ and that of the cylinder previously described $V_{cyl} = \pi\rho_{ap}^2 z_{ndr}$. It is easy to show that $\mathcal{G}_{3D} = (2\pi/3)C_\rho^2 C_z$. Interestingly, the boundaries obtained for $\mathcal{G}_{2D}$ also hold for $\mathcal{G}_{3D}$, hence the relation between $\mathcal{G}_{3D}$ and $\mathcal{G}_{2D}$ within the region of confinement is simply $\mathcal{G}_{3D} = (2\pi/3)C_\rho \mathcal{G}_{2D}$.

A closer look at the expression of $\mathcal{G}_{3D}$ raises a very interesting aspect: the axicon angle that maximizes the localization (minimizes $\mathcal{G}_{3D}$) is given by $\theta = 2\arctan(\sqrt{5-2\sqrt{6}}) \simeq 35°$, provided that $\theta_{low} < \theta < \theta_{up}$. This result is of fundamental importance since it furnishes a rule for optimizing the volumetric confinement of an X-wave regardless of the operating conditions of the launcher (i.e., fractional bandwidth, aperture radius, operating frequency), provided that the X-wave experiences negligible cone dispersion.

III. Energetic Properties

The discussion on the confinement properties of localized beams and pulses addressed so far was exclusively based on a geometrical argument. To complete the picture, energetic aspects have to be considered. While the energy efficiency of Bessel beams has already been commented in [25] (where it has also been compared to that of Gaussian beams), the energy efficiency of X-waves has not been analyzed, yet. For this purpose, we move from the considerations made in [25] and extend them to the context of X-waves. It is worth to stress here that in the *near-field* region (where X-waves notably exhibit their nondiffractive properties) it is not possible to gauge the energetic confinement of the fields through the directivity, as the latter figure of merit is defined only in the *far-field* region. However, it is important to measure the portion of the total energy of the pulse that is carried within its main spot. This problem naturally suggests the following definition of *energy metric*:

$$\mathcal{E}_{2D} = \frac{\iint_{R_0} |\chi|^2 \mathrm{d}x\mathrm{d}z}{\iint_{R} |\chi|^2 \mathrm{d}x\mathrm{d}z}. \tag{9}$$

Indeed, $\mathcal{E}_{2D}$ determines the fraction of the energy launched within the domain of interest (i.e., $R = \{(x, z); |x| \le \rho_{ap}, 0 \le z \le z_{ndr}\}$) that is contained within the first nulls (i.e., $R_0 = \{(x, z); |x| \le S_\rho/2, |z - z_{ndr}/2| \le S_z/2\}$).

Differently to the case of Bessel beams, analytic expressions for describing the X-wave intensity distribution over all the space are not available (on-axis expressions can be found, e.g., in [13]). However, (9) can be evaluated numerically, and it is reported as a contour plot over the $\bar{\rho}_{ap}\theta$ plane for the case $\Delta\bar{\omega} = 0.2$, as has been done for the confinement metric $\mathcal{G}_{2D}$. Again, cases when the spot-sizes $S_\rho(S_z)$ exceed $d_{ap}(z_{ndr})$ are of scarce interest, thus only values of the energy metrics within the conditions $C_\rho < 1$ and $C_z < 1$ are considered. Indeed, according to the definition of $\mathcal{E}_{2D}$ in (9), in the limiting case $C_\rho \to 1$ and $C_z \to 1$, it results $\mathcal{E}_{2D} \to 1$.

Numerical results (see Fig. 3(a)) reveal us that a higher geometrical confinement (lower $\mathcal{G}_{2D}$) of the X-wave does not

This article has been accepted for publication in a future issue of this journal, but has not been fully edited. Content may change prior to final publication. Citation information: DOI 10.1109/TAP.2019.2938628, IEEE Transactions on Antennas and Propagation

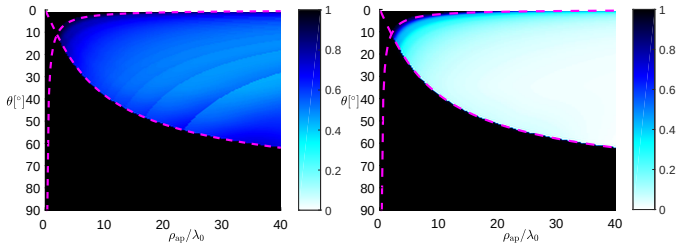

Fig. 3. The energy metric (a) $\mathcal{E}_{2D}$ and (b) $\mathcal{E}_{3D}$ vs. ρ_{ap}/λ_0 and θ as defined in (9) and (10), respectively. The fractional bandwidth of $\Delta\bar{\omega} = 0.2$ is assumed as in Fig. 2(a).

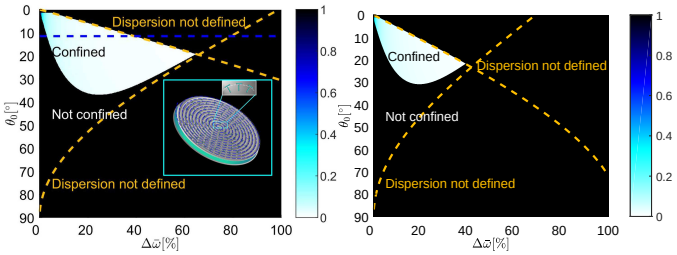

Fig. 4. Dispersive metrics $\mathcal{G}^{d}_{2D}$ for (a) $n_d \simeq 1.02$ and (b) $n_d \simeq 1.9$. In both cases the aperture radius is fixed to $\rho_{ap} = 15\lambda_0$. The blue dashed line in (a) represents the operating point of the example in [13] (see the inset), while the dashed orange lines represent the boundaries for which the cone dispersion is no longer defined (i.e., equation (14) and (15)).

necessarily correspond to a higher energy confinement (higher $\mathcal{E}_{2D}$). This aspect is a direct consequence of the definition of geometrical and energy metrics and the presence of tails of energy outside the main spot of any X-wave. Indeed, for a given θ, when $\bar{\rho}_{ap}$ increases the geometrical metric can only decrease according to the definition of $\mathcal{G}_{2D}$. On the other hand, the contributions of the tails with respect to the main spot might be no longer negligible, thus leading to a weaker energy efficiency.

We should stress here that a weaker energy efficiency is the price to pay for a higher localization, as also commented in [25] with reference to Bessel beams. There, it was pointed out that the energy efficiency of a Bessel beam goes as $1/N_z$, where N_z are the number of nulls achieved by the Bessel function at $\rho = \rho_{ap}$. This is fully consistent with the fact that the transverse behavior of a nondispersive X-wave recalls the one of a Bessel beam [13]. We also note that the numerical results of Fig. 3(a) confirm the accuracy of the approximation of S_ρ for an X-wave (note the excellent agreement between the discontinuity of the contour plot and the boundaries $C_\rho = 1$ and $C_z = 1$).

As for the geometric metric, we can extend the energy metric to account for the 3-D nature of the fields as well:

$$\mathcal{E}_{3D} = \frac{\iiint\limits_{E} |\chi|^2 \rho \mathrm{d}\rho \mathrm{d}\rho \mathrm{d}z}{\iiint\limits_{R} |\chi|^2 \rho \mathrm{d}\rho \mathrm{d}\rho \mathrm{d}z}, \tag{10}$$

where E is the elliptical domain delimited by the nulls, i.e., $E = \{(\rho, z); (2\rho/S_\rho)^2 + [2(z - z_{ndr})/S_z]^2 \leq 1\}$, whereas R is defined as in (9) upon replacing $|x|$ with ρ. This definition comes from a straightforward generalization of (9) to a volume integral where the azimuthal symmetry of X-waves is exploited, thus leading to a surface integral. As a result, (9) and (10) only differ for the Jacobian of the transformation (viz., ρ), and the domain E of the integral at numerator.

The analysis of the numerical results of $\mathcal{E}_{3D}$ (see Fig. 3(b)) reveals a very important aspect: the minimum of $\mathcal{E}_{3D}$ for $\theta_{low} < \theta < \theta_{up}$ is achieved for $\theta \simeq 35°$, regardless of $\bar{\rho}_{ap}$. This is the same result obtained for the geometric metric $\mathcal{G}_{3D}$. Therefore, we can conclude that the geometric metrics defined in Section II provide for approximate still accurate figures of merit for the analysis of the confinement properties of X-waves.

IV. Dispersive Properties

All results presented so far hold for a nondispersive X-wave. From now on, we aim at qualitatively and quantitatively assess the effect of cone dispersion in the focusing features of dispersive X-waves. The first issue that arises when dealing with dispersive X-waves is the definition of a suitable metric of confinement. Indeed, when dispersion comes into play, the X-wave slightly spreads as it propagates, thus S_ρ and S_z are functions of z and t. However, it has been shown in [13] that the main spot remains almost constant within a nondiffracting distance that is now given by $z'_{ndr} = \rho_{ap} \cot\theta_M$, where θ_M is the maximum angle assumed by the cone dispersion within the considered frequency bandwidth i.e, $\theta(\omega) \leq \theta_M$, for $|\omega - \omega_0| < \Delta\omega/2$. In addition, in the dispersive case the spot sizes are well approximated by those of a nondispersive X-wave with axicon angle evaluated at the central frequency $\theta_0 = \theta(\omega_0)$ [13]. As a result, the confinement ratios for a dispersive X-wave take the following approximate expressions

$$C^{d}_{\rho} = \frac{j_{0,1}}{2\pi\bar{\rho}_{ap}\sin\theta_0}, \; C^{d}_{z} = \frac{2\tan\theta_M}{\bar{\rho}_{ap}\Delta\bar{\omega}\cos\theta_0}. \tag{11}$$

Therefore, the geometric metric for *dispersive* X-waves $\mathcal{G}^{d}_{2D}$ is still given by (7), with the formal change $C_\rho(C_z) \to C^{d}_{\rho}(C^{d}_{z})$.

Clearly, θ_M depends on θ_0, $\Delta\bar{\omega}$ and $\theta(\omega)$, i.e., the functional dependence of the cone dispersion. Specifically, for dielectric-filled radial waveguides (n_d being the refractive index of a lossless dielectric filling) the functional dependence of the cone dispersion is well approximated [12] by the following analytic expression (equivalent to [13, eq. (24)]):

$$\theta(\omega) = \arcsin\left[(\omega_0/\omega)(\sin\theta_0 + n_d) - n_d\right], \tag{12}$$

thus θ_M is achieved at $\omega = \omega_0 - \Delta\bar{\omega}/2$ and reads

$$\theta_M = \arcsin\left[(\sin\theta_0 + n_d)/(1 - \Delta\bar{\omega}/2) - n_d\right]. \tag{13}$$

We note that the minimum angle θ_m assumed by the cone dispersion within the considered bandwidth is achieved at $\omega = \omega_0 + \Delta\bar{\omega}/2$, thus its expression is given by (13), apart for a sign change of the term $\Delta\bar{\omega}/2$.

In order to analyze the effect of cone dispersion, we consider the cases of a radial waveguide filled with a dielectric foam ($n_d \simeq 1.02$), and one filled with a glass-like material, ($n_d \simeq 1.9$), as shown in Figs. 4(a) and (b), respectively. In both

cases the aperture radius is fixed to $\rho_{\rm ap} = 15\lambda_0$. (An example of such a dispersive radial waveguide is shown in the inset of Fig. 4(a).) For these two case studies, it is interesting to represent $\mathcal{G}_{\rm 2D}^{\rm d}$ as a 2-D function of θ_0 and $\Delta\bar{\omega}$ (see Figs. 4(a) and (b)). Interestingly, the inspection of Figs. 4(a) and (b) reveals that the localization properties of such X-wave launchers not always improve with an increase of the fractional bandwidth, but they strictly depend on the choice of the operating axicon angle θ_0 and of the dielectric filling.

As can be expected, for higher refractive indexes (see Fig. 4(b)) cone dispersion is more prominent and, as a result, one has a restricted choice of possible operating axicon angles and fractional bandwidths to obtain a spatially-confined X-wave. As opposed to nondispersive X-waves, the fractional bandwidth that optimizes the confinement of the main spot is no longer the largest one [13]. In this regard, we should note here that θ_0 and $\Delta\bar{\omega}$ cannot take arbitrary values, but they are constrained by $\theta_{\rm M} < 90^\circ$ and $\theta_{\rm m} > 0^\circ$. These two conditions defines an upper $\theta_{0,\rm up}$ and a lower boundary $\theta_{0,\rm low}$ to θ_0 (represented as dashed orange lines in Figs. 4(a) and (b)) given by

$$\theta_{0,\rm up} = \arcsin\left[1 - \Delta\bar{\omega}(1+n_{\rm d})/2\right], \tag{14}$$

$$\theta_{0,\rm low} = \arcsin\left[\Delta\bar{\omega}n_{\rm d}/2\right]. \tag{15}$$

Equating (14) and (15) yields the crossing point:

$$\Delta\bar{\omega}_{\rm c} = 2(1-\sin\theta_0)/(1+n_{\rm d}), \tag{16}$$

$$\theta_{0,\rm c} = \arcsin\left(n_{\rm d}/(1+2n_{\rm d})\right). \tag{17}$$

The importance of these expressions is readily explained. Indeed, $\Delta\bar{\omega}_{\rm c}$ dictates a fundamental theoretical limit to the maximum fractional bandwidth over which a dispersive pulse can be generated through a radial waveguide, whereas $\theta_{0,\rm c}$ is the operating axicon angle for which the widest fractional bandwidth can theoretically be achieved. However, the operating point given by these two theoretical limits is solely based on the dispersion relation of a radial waveguide. Conversely, when the confinement metric of a localized wave is taken into account, for any given θ_0 there exists a minimum $\Delta\bar{\omega}_{\rm m}$ and a maximum $\Delta\bar{\omega}_{\rm M}$ fractional bandwidth for which confinement is possible. Such extremal values can be found by searching for the roots of the algebraic equation (see Appendix) given by $C_z^{\rm d} = 1$, once $\bar{\rho}_{\rm ap}$, $n_{\rm d}$, and θ_0 are fixed (provided that $\theta_{0,\rm low} < \theta_0 < \theta_{0,\rm up}$). To give some numbers, for the case analyzed in [9], [13] the minimum and the maximum fractional bandwidth would approximately be 3%, and 38% (see the intersections between the blue dashed line and the dark region in Fig. 4(a)), respectively.

Finally, one would be interested to find the operating axicon angle that leads to the widest fractional bandwidth within the confinement region. Although such an operating point cannot be expressed in analytical closed-form, it should be noted that $\Delta\bar{\omega}_{\rm c}$ and $\theta_{0,\rm c}$ as given by (16), (17), respectively, provide a very good approximation of such an optimal point (see in Figs. 4(a)–(b), how the confined region (bright colors) extends close to the crossing point (intersection of dashed orange lines)).

V. Conclusion

In this work we have obtained analytical expressions for describing the *geometric confinement* of Bessel beams and X-waves. Formulas have been provided for the optimal choice of the axicon angle to design highly-confined Bessel beams and X-waves. Moving from this geometrical argument, we have also numerically analyzed the *energy confinement* of nondispersive X-waves. This analysis highlights the correspondence between geometric and energy confinements. Finally, the relevant case of dispersive X-waves has been addressed considering the typical wavenumber dispersion of radial waveguides. In this case, a suitable metric of confinement has been defined, and further design criteria have been provided. In particular, as a relevant difference with respect to nondispersive X-waves, it is found that the localization of a dispersive X-wave generated through a radial waveguide does not improve for the largest possible fractional bandwidth. Conversely, upper and lower bounds exist, depending on both the operating axicon angle and the dielectric filling the waveguide.

Acknowledgments

We wish to acknowledge Mauro Ettorre, Alessandro Galli, Matteo Albani, and Guido Valerio for stimulating discussions.

Appendix

The condition $C_z^{\rm d} = 1$ defines an algebraic equation in terms of θ_0 and $\Delta\bar{\omega}$:

$$\frac{2\tan\theta_{\rm M}}{\Delta\bar{\omega}\bar{\rho}_{\rm ap}\cos\theta_0} = 1, \tag{18}$$

where $\theta_{\rm M}$ can be expressed in terms of θ_0 and $\Delta\bar{\omega}$ through (13) leading to

$$\tan\theta_{\rm M} = \frac{\Delta\bar{\omega}n_{\rm d} + 2\sin\theta_0}{\sqrt{(2-\Delta\bar{\omega})^2 - (\Delta\bar{\omega}n_{\rm d} + 2\sin\theta_0)^2}}. \tag{19}$$

Using (19) in (18) yields

$$(\Delta\bar{\omega}\bar{\rho}_{\rm ap}\cos\theta_0)^2[(2-\Delta\bar{\omega})^2 - (\Delta\bar{\omega}n_{\rm d} + 2\sin\theta_0)^2] = 4(\Delta\bar{\omega}n_{\rm d} + 2\sin\theta_0)^2\tan\theta_{\rm M}. \tag{20}$$

After simple algebraic manipulations, (20) can be rewritten as a quartic equation of the variable $\Delta\bar{\omega}$

$$a\Delta\bar{\omega}^4 + b\Delta\bar{\omega}^3 + c\Delta\bar{\omega}^2 + d\Delta\bar{\omega} + e = 0, \tag{21}$$

with coefficients:

$$\begin{aligned} a &= \bar{\rho}_{\rm ap}^2\cos^2\theta_0(1-n_{\rm d}^2)/4,\\ b &= -\bar{\rho}_{\rm ap}^2\cos^2\theta_0(1+n_{\rm d}\sin\theta_0),\\ c &= \bar{\rho}_{\rm ap}^2\cos^4 - n_{\rm d}^2,\\ d &= -4n_{\rm d}\sin\theta_0,\\ e &= -4\sin^2\theta_0. \end{aligned} \tag{22}$$

As is well known, (22) admits a general solution, but its expression is cumbersome and thus not reported. Nevertheless, the roots of (22) can easily be found numerically, once $\bar{\rho}_{\rm ap}$, $n_{\rm d}$ and θ_0 are fixed. Finally, the two extremal values of the fractional bandwidths are found by searching for the two positive roots (among the possible four) of (22), provided that $\theta_{0,\rm low} < \theta_0 < \theta_{0,\rm up}$.

REFERENCES

[1] M. Ettorre, S. C. Pavone, M. Casaletti, M. Albani, A. Mazzinghi, and A. Freni, "Near-field focusing by non-diffracting Bessel beams," in *Aperture Antennas for Millimeter and Sub-Millimeter Wave Applications*. Cham, Switzerland: Springer, 2018, pp. 243–288.

[2] H. E. Hernández-Figueroa, M. Zamboni-Rached, and E. Recami, *Non-diffracting Waves*. Weinheim, Germany: John Wiley & Sons, 2013.

[3] D. McGloin and K. Dholakia, "Bessel beams: diffraction in a new light," *Contemporary Phys.*, vol. 46, no. 1, pp. 15–28, 2005.

[4] R. M. Herman and T. A. Wiggins, "Production and uses of diffractionless beams," *J. Opt. Soc. Am. A*, vol. 8, no. 6, pp. 932–942, 1991.

[5] S. Monk, J. Arlt, D. A. Robertson, J. Courtial, and M. J. Padgett, "The generation of Bessel beams at millimetre-wave frequencies by use of an axicon," *Opt. Commun.*, vol. 170, no. 4, pp. 213–215, 1999.

[6] M. Ettorre, S. M. Rudolph, and A. Grbic, "Generation of propagating Bessel beams using leaky-wave modes: experimental validation," *IEEE Trans. Antennas Propag.*, vol. 60, no. 6, pp. 2645–2653, 2012.

[7] W. Fuscaldo, G. Valerio, A. Galli, R. Sauleau, A. Grbic, and M. Ettorre, "Higher-order leaky-mode Bessel-beam launcher," *IEEE Trans. Antennas Propag.*, vol. 64, no. 3, pp. 904–913, 2016.

[8] M. Ettorre, S. C. Pavone, M. Casaletti, and M. Albani, "Experimental validation of Bessel beam generation using an inward Hankel aperture distribution," *IEEE Trans. Antennas Propag.*, vol. 63, no. 6, pp. 2539–2544, 2015.

[9] S. C. Pavone, M. Ettorre, and M. Albani, "Analysis and design of Bessel beam launchers: Longitudinal polarization," *IEEE Trans. Antennas Propag.*, vol. 64, no. 6, pp. 2311–2318, 2016.

[10] B. G. Cai, Y. B. Li, W. X. Jiang, Q. Cheng, and T. J. Cui, "Generation of spatial Bessel beams using holographic metasurface," *Opt. Express*, vol. 23, no. 6, pp. 7593–7601, 2015.

[11] D. Comite, W. Fuscaldo, S. K. Podilchak, P. D. H. Re, V. Gómez-Guillamón Buendía, P. Burghignoli, P. Baccarelli, and A. Galli, "Radially periodic leaky-wave antenna for Bessel beam generation over a wide-frequency range," *IEEE Trans. Antennas Propag.*, vol. 66, no. 6, pp. 2828–2843, 2018.

[12] S. C. Pavone, A. Mazzinghi, A. Freni, and M. Albani, "Comparison between broadband Bessel beam launchers based on either Bessel or Hankel aperture distribution for millimeter wave short pulse generation," *Opt. Express*, vol. 25, no. 16, pp. 19 548–19 560, 2017.

[13] W. Fuscaldo, S. C. Pavone, G. Valerio, A. Galli, M. Albani, and M. Ettorre, "Analysis of limited-diffractive and limited-dispersive X-waves generated by finite radial waveguides," *J. App. Phys.*, vol. 119, no. 19, p. 194903, 2016.

[14] W. Fuscaldo, D. Comite, A. Boesso, P. Burghignoli, P. Baccarelli, and A. Galli, "Focusing leaky waves: A class of electromagnetic localized waves with complex spectra," *Phys. Rew. App.*, vol. 9, no. 5, p. 054005, 2018.

[15] D. Comite, W. Fuscaldo, S. Podilchak, V. Gómez-Guillamón Buendía, P. Hilario Re, P. Baccarelli, P. Burghignoli, and A. Galli, "Microwave generation of X-waves by means of a planar leaky-wave antenna," *Applied Physics Letters*, vol. 113, no. 14, p. 144102, 2018.

[16] J. Durnin, "Exact solutions for nondiffracting beams. I. The scalar theory," *J. Opt. Soc. Am. A*, vol. 4, no. 4, pp. 651–654, 1987.

[17] P. Saari and K. Reivelt, "Evidence of X-shaped propagation-invariant localized light waves," *Phys. Rev. Lett.*, vol. 79, no. 21, p. 4135, 1997.

[18] N. Chiotellis, V. Mendez, S. M. Rudolph, and A. Grbic, "Experimental demonstration of highly localized pulses (X waves) at microwave frequencies," *Phys. Rev. B*, vol. 97, no. 8, p. 085136, 2018.

[19] H. Sonajalg and P. Saari, "Suppression of temporal spread of ultrashort pulses in dispersive media by Bessel beam generators," *Opt. Lett.*, vol. 21, no. 15, pp. 1162–1164, 1996.

[20] M. A. Porras, G. Valiulis, and P. Di Trapani, "Unified description of Bessel X waves with cone dispersion and tilted pulses," *Phys. Rev. E*, vol. 68, no. 1, p. 016613, 2003.

[21] J. Durnin, J. J. Miceli Jr., and J. H. Eberly, "Diffraction-free beams," *Phys. Rev. Lett.*, vol. 58, no. 15, p. 1499, 1987.

[22] G. N. Watson, *A Treatise on the Theory of Bessel Functions*. Cambridge, UK: Cambridge University Press, 1995.

[23] M. Born and E. Wolf, *Principles of Optics*. Cambridge, UK: Cambridge University Press, 1997.

[24] W. Fuscaldo, S. C. Pavone, D. Comite, G. Valerio, M. Albani, M. Ettorre, and A. Galli, "Design criteria of x-wave launchers for millimeter-wave applications," in *Eur. Conf. Antennas Propag.*, 9–13 Apr. 2018, London, UK, 2018.

[25] J. Durnin, J. H. Eberly, and J. J. Miceli Jr., "Comparison of Bessel and Gaussian beams," *Opt. Lett.*, vol. 13, no. 2, pp. 79–80, 1988.